Observation of Cryogenic Hydrogen Pellet Ablation with a Fast-frame Camera System in the TJ II Stellarator

N. Panadero, K. J. McCarthy, E. de la Cal, J. Hernández Sánchez, R. García, M. Navarro and TJ-II team
Laboratorio Nacional de Fusión, CIEMAT, Madrid, Spain

Introduction

Plasma core fuelling is critical for the development of steady state operation in large fusion devices, especially in helical type reactors [1]. The usual refuelling method, gas puffing, will not be useful for such large devices, since the fuel reaching the core is minimal. At present, cryogenic pellet injection is the most promising technique for efficient core fuelling. Moreover, pellets can be injected to suppress instabilities, to modify density and temperature profiles, and as an active diagnostic [2]. However, a complete comprehension of the physics of pellet ablation and subsequent particle transport (drift/diffusion) remains outstanding and thus ongoing studies are required. A pellet is ablated by background plasma particles so the ablated material forms an expanding cloud of neutrals that will become partially ionized eventually and will expand along the magnetic field lines. Moreover, the ablatant shields the pellet from ambient plasma in a self-regulated manner [3]. The understanding of pellet ablation can allow better mass deposition control and, therefore, improved plasma refuelling. In this work, the experimental set-up and capabilities of the TJ-II pellet injection system are briefly described. Next, fast-camera images are analysed for a range of pellet types injected into several plasmas. Finally, observed pellet toroidal deflection and future work are discussed.

Experimental set-up

TJ-II is a 4-period, low magnetic shear stellarator with a major radius of 1.5 m and average minor radius ≤0.22 m [4]. A set of poloidal, toroidal and vertical coils creates a fully 3-D magnetic-field with bean shaped cross section and B(0)≤1 T. Electron Cyclotron Resonance Heating (ECRH) and/or Neutral Beam Injection (NBI) are used. Central electron densities, $n_e(0)$, up to 1.7×10^{19} m^{-3}, and temperatures, $T_e(0)$, up to 1 keV are attained with ECRH. Co- and counter NBIs provide up to 1 MW of additional heating, which leads to $n_e(0) \leq 5\times10^{19}$ m^{-3} and $T_e(0) \leq 300$ eV (with lithium coating on the vacuum vessel wall).

TJ-II is equipped with a pellet injector (PI) [5, 6] that can provide up to four hydrogen pellets of different sizes per discharge, with between ~3.1×10^{18} and ~4.2×10^{19} H atoms/pellet. Once formed, a fast solenoid valve based propulsion system accelerates a pellet into TJ-II at ~800 m/s to ~1200 m/s. In addition the PI possesses an in-line diagnostic system which includes a light-gate (light emitting and light sensitive diode that provide a time signal) and a microwave

cavity mass detector that provides a mass dependent time signal. These signals are used for velocity and mass determination. In addition, an optical fibre based diagnostic system is used to record the Balmer H_α light (λ = 656.28 nm) emitted by the neutral cloud. Amplified silicon photodiodes with H_α filters are located in two nearby viewport to follow the evolution of the temporal evolution of H_α light from above (TOP) and behind (SIDE). Pellet positions and ablation rates are determined assuming that a pellet is not accelerated and that H_α emission is proportional to ablation rate. Note: H_α signals are corrected for light collection solid angle, collection angle with respect to the fibre normal, interference filter transmission, detector efficiency and amplifier gain. These corrections allow a comparison of modelled ablation rates with H_α emission, even though the number of H_α photons/particle is unknown. Besides, an ultra-fast CMOS camera (APX-RS by Photron Ltd.), capable of recording up to 250 kfps (128x16 pixels) with an exposure time ≥1 μs, is located directly above the pellet flight path. See Fig. 1. It is equipped with a coherent fibre bundle and a machine-vision type camera lens (HF12.5SA-1 by Fujinon). Images are used to study pellet deflection and acceleration, plus cloud shape, asymmetry, drift and elongation along magnetic field lines [7].

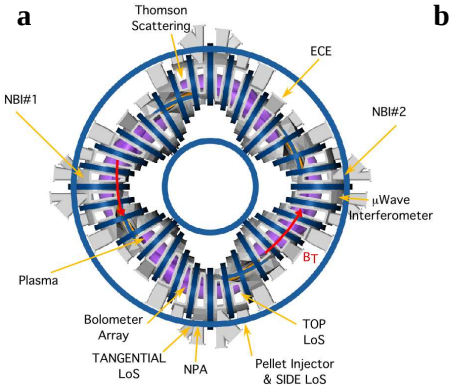

Figure 1: a) Bird's eye view of the TJ-II showing the location of the PI, the fast camera and the NBI injection directions b) TJ-II sector B2 with pellet flight path, a standard bean-shaped magnetic configuration plus fast-camera, TOP and SIDE photodiode view angles.

Results

In this study, three TJ-II discharges, with different heating methods and similar pellet sizes, are considered. Fast camera images for the three cases are shown in Fig. 2. A comparison between the H_α (TOP) signals and the light intensity profiles recorded by the fast-camera are shown in Fig. 3. In these cases, pellet toroidal deflection is observed when heating with either NBI#1 (co-counter) or NBI#2 (counter) but not with ECRH. Next, pellet trajectories are plotted together with estimated pellet toroidal velocities in Fig. 4. It is apparent that toroidal deflections are comparable for both NBIs but negligible for ECRH plasmas. The characteristics of the hydrogen NBIs are given in Table 1. The ratios of the three energy components: E, E/2 and E/3, is typically 55:25:20 [8].

#Shot	NBI	P (kW)	V(kV)	I(A)
41107	1	500	31	52.5
41391	2	340	28	44.5

Table 1. NBI injected powers, acceleration voltages and injected currents for #41107 and #41391.

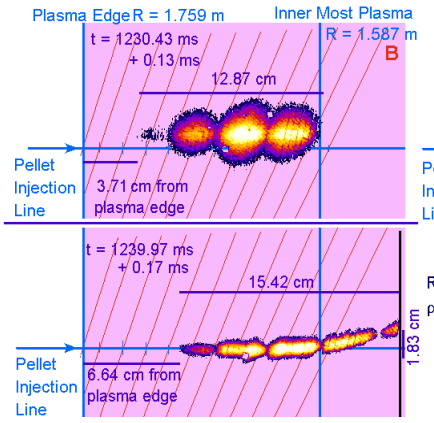

Figure 2. Fast camera images of Type-2 pellets injected into ECRH and ECRH+NBI plasmas created with magnetic configuration 100_44_64. Pellet and plasma details are found in Table. 2

#Shot	Heating	#H atoms (10^{18} ± 20%)	Velocity (ms^{-1})	$\bar{n}_{e,bef}$ (10^{19} m^{-3})	Lens (mm)	Iris	Frame rate (kfps)	τ_{exp} (μs)
41016	ECRH	5	997.27	0.4	12.5	f/11	30	33.3
41107	ECRH+NBI1	6.7	1062.3	2.2	12.5	f/8	30	33.3
41391	ECRH+NBI2	6.5	1089.7	2.8	12.5	f/8	37	27

Table 2. Pellet and plasma characteristics, along with fast camera parameters.

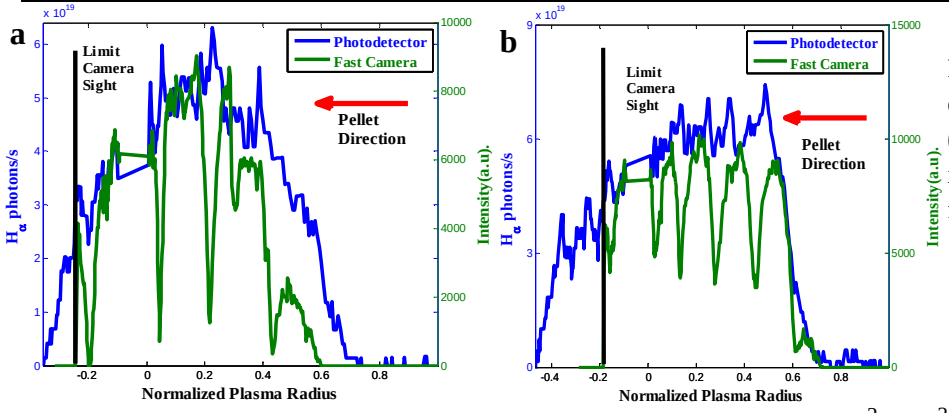

Figure 3. Comparisons of H_α detected by TOP (blue) and light intensity profile from fast camera (green) for:
a) 41107
b) 41391

Average pellet toroidal velocities are found to be in the range of 10^2 - 10^3 m s^{-1}, while toroidal accelerations lie between 10^6 - 10^7 m s^{-2}. It is postulated that the observed deflections are due to momentum exchange with NBI fast ions, since heating asymmetry, responsible for the rocket effect, is estimated to be a minor effect here, (see Fig. 2). With regard to momentum exchange, toroidal acceleration is found to be in the range of 10^5 – 10^8 ms^{-2}. On the other hand, the toroidal acceleration due to rocket effect is in the range 10^5 – 10^6 ms^{-2}.

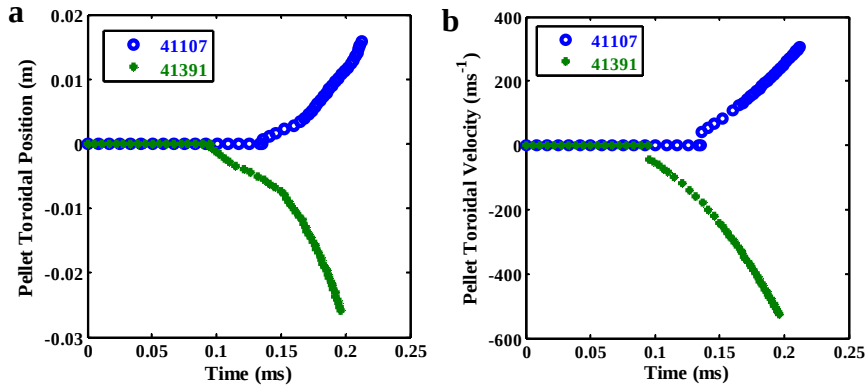

Figure 4. a) Toroidal pellet position and b) velocity for #41107 (blue) and #41391(green) as a function of time after reaching plasma edge.

Total deflection is found to be significantly dependent on plasma density, (see Fig. 5). This may be explained considering that fast particle capture from the NBIs depends on electron

density. For instance, for low-density plasmas beam absorption is minimal in the plasma core while there is little fast-ion slowdown [9]; for medium-density plasmas, high beam absorption takes place in the core while fast-ion slowdown is enhanced; for high densities, beam absorption increases at external plasma radii and fast-ion slowdown is maximum.

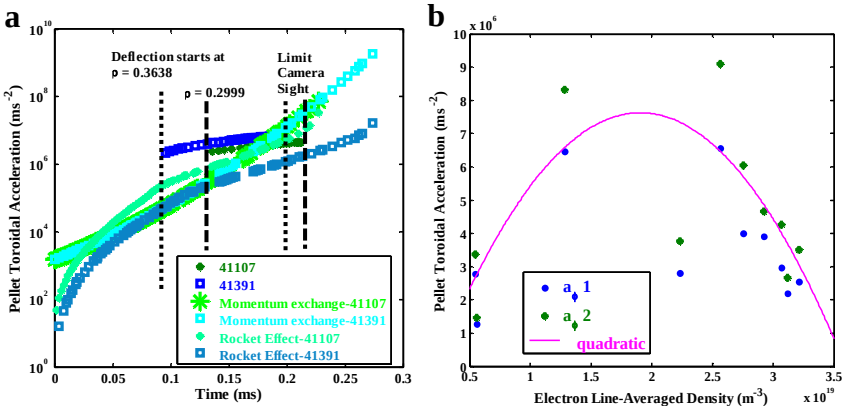

Figure 5. a) Toroidal acceleration from fast camera images, momentum exchange [3, 10] and rocket effect [11] for 41107 (green) and 41391 (blue) b) Variation of pellet toroidal acceleration with plasma line-averaged density.

Conclusions

Trajectories of pellets injected into TJ-II have been analysed in two dimensions. Toroidal deflections are found to be in the range of 10^6 - 10^7 ms^{-2} for unbalanced NBI plasmas, both co- and counter injections. Moreover, deflection depends on plasma density. In contrast, while radial acceleration is not observed, poloidal deflection cannot be study with this system, though it is predicted that pellets should deviate in the poloidal direction. The dependence of pellet deflection on both plasma density and NBI direction requires further studies.

This work has been carried out within the framework of the EUROfusion Consortium and has received funding from the Euratom research and training programme 2014-2018 under grant agreement No 633053. The views and opinions expressed herein do not necessarily reflect those of the European Commission. In addition, it is partially financed by a grant from the Spanish Ministerio de Ciencia y Innovación (Ref. ENE2013-48679-R).

[1] H. Maaßberg et al., Plasma Phys. Control. Fusion 41 (1999) 1135.

[2] B. Pégourié, Plasma Phys. Control. Fusion 49 (2007) R87-R160.

[3] P. B. Parks et al., Nucl. Fusion 17 (1977) 539.

[4] J. Sánchez et al., Nucl. Fusion 49 (2009) 104018.

[5] S. K. Combs et al., Fusion Sci. Tech. 64 (2013) 513.

[6] K. J. McCarthy et al., Proc. Sci. (ECPD2015) 134.

[7] G. Kocsis et al., Rev. Sci. Instrum., 75 (2004) 4754.

[8] K. J. McCarthy et al. J. Physics B: Atomic, Molecular and Optical Physics 43 (2010) 144020.

[9] A. Bustos, Nucl. Fusion 51 (2011) 083040.

[10] Y. Nakamura et al., Nucl. Fusion 26 (1986) 907.

[11] J.S. Mishra et al., Nucl. Fusion 51 (2011) 083039.